Title:
Improvement in bonding strength by applying circumferential sliding in cold copper/aluminum forge-bonding

Authors:
Ryo Matsumoto[1,*], Kakeru Hashimoto[1] and Hiroshi Utsunomiya[1]

* Correspnding author (R. Matsumoto, E-mail: ryo@mat.eng.osaka-u.ac.jp, Tel: +81-6-6879-7500, Fax: +81-6-6879-7500)

Affiliation:
[1] Division of Materials and Manufacturing Science, Osaka University, 2-1 Yamadaoka, Suita 565-0871, Japan

Abstract

To improve bonding characteristics of two dissimilar workpieces in cold forge-bonding, a processing parameter of circumferential sliding with respect to the forging axis on the contact interface was considered. In this forge-bonding process, stacked cylindrical workpieces of copper (upper) and aluminum (lower) were simultaneously backward-extruded into a cup shape between upper and lower punches. The upper punch was moved down along the forging axis, while the lower punch was rotated with respect to the forging axis. Forging speed was 0.1 mm/s, while circumferential sliding was applied by the lower punch with a rotation speed of maximum 1.5 rpm and a rotation angle of maximum 590° on the contact interface. Circumferential sliding did not change the geometrical profile and surface expansion of the contact interface, while it promoted bonding of aluminum on copper. As a result, the workpieces were bonded with approximately 25% shorter in the forging stroke and four times higher in the bonding strength at the same forging stroke. The maximum nominal bonding strength was approximately 30 MPa under a punch rotation angle of 590°.

Keywords: Joining; Forging; Extrusion; Circumferential sliding; Dissimilar materials

1. Introduction

Lightweight and high-strength are vital factors for structural components, especially in the transportation section. Furthermore, high-functional characteristics such as vibration absorption and corrosion resistance, are strongly desired. To achieve such advanced structural components, optimal materials having desirable properties are selected and combined. In manufacturing of ideal multi-material components, joining process such as welding and threaded fastener of dissimilar materials, is essential (Martinsen et al., 2015). Joining process using plastic deformation is also applied in producing multi-material components (Groche et al., 2014a). In plastic joining process, mechanical joining such as self-pierce riveting (Mori et al., 2013), and metallurgical bonding such as friction stir welding (Cai et al., 2019), are major methods in plastic joining with dissimilar materials.

Since solid phase welding by plastic deformation (cold plastic joining) does not require heating process, high productivity and low manufacturing energy are easily realized. Moreover, joining part is free from embrittlement and thermal strain which occur from thermal history. Thus, various forging and extrusion techniques have been proposed in cold plastic joining processes with dissimilar materials. For joining of steel and aluminum, Napierala et al. (2019) proposed draw-forging process, while Miwada et al. (2014) proposed forge spot-bonding process. Klaus and Merklein (2020) investigated joining of dissimilar materials by cold formed pin-structure. Zebardast and Taheri (2011) joined a rod with aluminum core and copper sheath using equal channel angular extrusion (ECAE) process, while Plancak et al. (2012) joined a rod component with copper core and aluminum sheath by forward extrusion. Yoshida et al. (2012b) investigated bonding conditions of steel and aluminum in backward extrusion forge-bonding. Groche et al. (2014b) investigated the effects of preliminary heat treatment on the bond formation of steel and aluminum in backward

extrusion forge-bonding. The joining mechanism in these cold joining processes is mainly due to seizure by breaking up of oxide film and exposure of virgin surface of metals on the contact interface. In some cases, heat treatment is performed after cold joining, with the aim of strengthening the bonding of two materials by means of diffusion. Bay (1979) investigated the bonding strength in cold pressure welding under plane strain compression, and clarified the bonding mechanism under such conditions.

In joining of dissimilar materials with cold pressure welding (Ohashi and Hashimoto, 1978) and cold roll bonding (Bay et al., 1994), it has been reported that the bonding strength and bondability are improved by increasing the relative sliding on the contact interface. As stated earlier, this is mainly the results of breakup of oxide film and exposure of virgin surface promoted by the increase of the relative sliding. Although simply increasing the relative sliding improves the bonding characteristics in cold forge-bonding, it is generally accompanied by the change in forged shape. In order to maintain the forged shape and to increase the bonding strength at the same time, moderate circumferential sliding with respect to the forging axis may be an effective option.

In this study, with the aim of improving bondability and bonding strength in cold forge-bonding, circumferential sliding with respect to the forging axis is applied on the contact interface of dissimilar materials during forge-bonding. The influence of circumferential sliding on the bonding characteristics is investigated by the experiment of cold forge-bonding process with copper and aluminum workpieces. Finally, the mechanism of the change in bonding characteristics is discussed.

2. Experimental and analysis conditions

2.1. Backward extrusion forge-bonding conditions

Figure 1 shows the schematic illustrations of the die layout, the punch shape, the

surface groove of the punches and forged workpieces in backward extrusion forge-bonding. Two cylindrical workpieces with same diameter stacked in the z direction (the forging direction or height direction) were located on the lower (knockout) punch inserted in the container. The upper (extrusion) punch was moved down in the -z direction for backward extrusion of the workpieces. Simultaneously the lower punch was rotated in the θ direction (the circumferential direction) with respect to the z-axis. As a result, the workpieces were backward-extruded into a cup shape.

It was suitable to plastically deform both upper and lower workpieces in this forge-bonding. The plastic deformation behavior of the workpieces was affected by the combinations of material strength and initial height of the workpieces. The behavior was preliminary investigated under several combinations by the finite element analysis and experiment of forge-bonding. The yield (proof) stress ratio of the upper/lower workpiece of higher than approximately 1.8 and the initial height ratio of the upper/lower workpiece of approximately 0.5–1.5 were suitable. On the basis of the preliminary investigations, drawn bars of JIS C1100-O copper (>99.90 mass% Cu) and JIS A1070-O aluminum (>99.70 mass% Al) were used as initial materials of upper and lower workpieces for forge-bonding. The initial workpieces were machined to cylindrical shapes with ϕ13.9 mm in diameter and 5.0 mm (copper) and 7.0 mm (aluminum) in heights. The height direction of the workpieces was paralleled to the drawing direction of the bars. The copper and aluminum bars were each annealed at temperatures of 1123 K and 623 K for 1 hour before machining. The mean hardness of the annealed bars was 73 HV0.2 of copper and 37 HV0.2 of aluminum. The oxide film was removed from the contact surfaces of the workpieces as much as possible by polishing. The bottom surface of the copper workpiece and the top surface of the aluminum workpiece were polished with #400 emery paper under wet condition just before forge-bonding. The surface roughness of the workpieces was Ra = 0.40–0.60 μm on the end

surface after polishing.

Dies were made of JIS SKH51 high-speed tool steel (63 HRC). The contacting surfaces on the workpiece of the dies other than the end surface of the punches were polished to mirror-like finish (Ra = 0.02–0.03 μm). The knurled grooves were machined on the bottom end surface of the upper punch and the top end surface of the lower punch to grip the workpieces. The depth, vertical angle, cross angle and pitch of the knurled grooves were 0.4 mm, 60°, 120° and 0.8 mm, as shown in **Figure 1(c)**. On the inner diameter of the container, mineral oil with a kinematic viscosity of 32 mm^2/s at a temperature of 313 K was applied before forge-bonding.

For the upper punch, the speed was set to 0.1 mm/s, with the stroke (s) of 0–9.1 mm in forging direction. On the other hand, the lower punch was set to the rotation speed (ω) of 0–1.5 rpm, and cumulative rotation angle (θ_{cum}) of 0–590°. Owing to the knurled grooves on the surface of the lower punch, the lower workpiece was rotated without slipping at the interface of the lower punch–bottom of the lower workpiece. However, a large circumferential slip between the lower punch and the lower workpiece occurred at $\omega > 1.5$ rpm. This was due to the limitation of the grip force by the knurled grooves. The circumferential sliding at the upper–lower workpieces interface was difficult to be identified under the circumferential slipping of the punch–workpiece interface. Hence, the rotation speed of the lower punch was limited to ω = 0–1.5 rpm. Forge-bonding was carried out at room temperature. The extrusion ratio was 1.7 (the inner diameter of the container: ϕ14.0, the diameter of the upper punch: ϕ9.0).

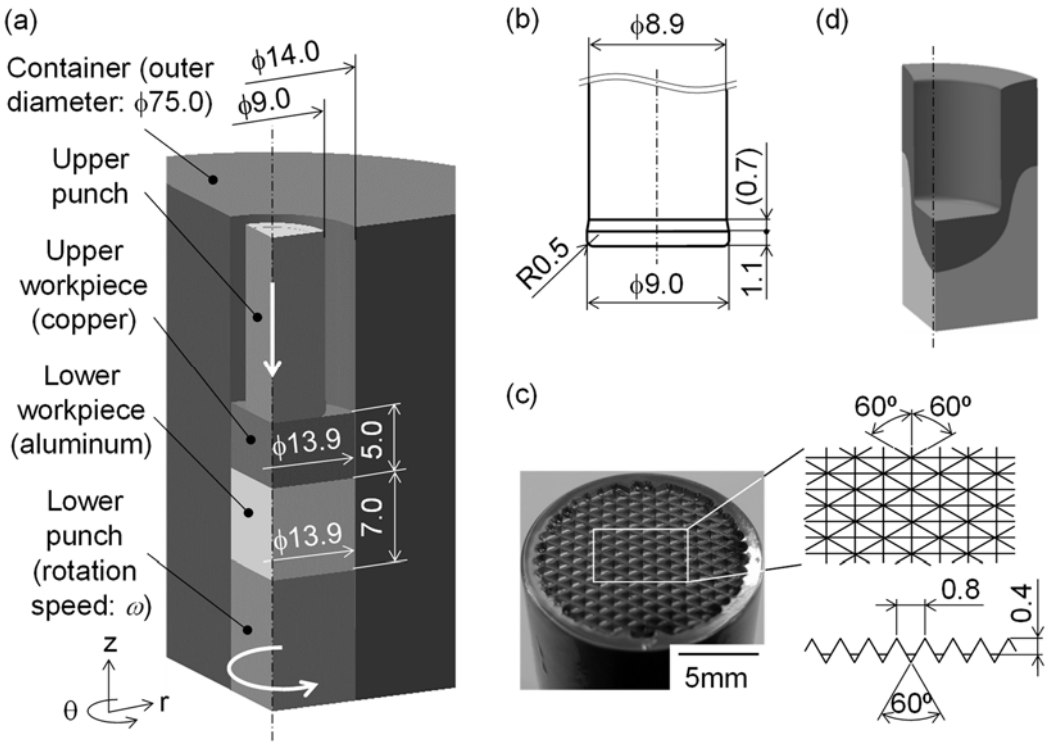

Fig. 1 Schematic illustrations of (a) die layout, (b) end shape of upper punch, (c) knurled grooves in end surface of punches and (d) forged workpieces (forging stroke s = 5.0 mm) in backward extrusion forge-bonding with circumferential sliding.

2.2. Experimental conditions of tensile test

The bonding strength between the forge-bonded upper and lower workpieces was measured by performing uniaxial tensile test on a material testing machine. First, the forge-bonded workpiece was sliced to a thickness of 2.0 mm in the center of the rθ cross section in parallel with the z-axis as shown in **Figure 2**. Next, the forge-bonded workpiece was tensiled with gripping the upper (copper) and lower (aluminum) parts, with a rate of 1 mm/min at room temperature.

The nominal bonding strength of the forge-bonded workpiece was identified by dividing the maximum tensile load by the nominal projected area of the rθ cross section of the forge-bonded workpiece (14 mm in length of radial direction and 2.0 mm in thickness).

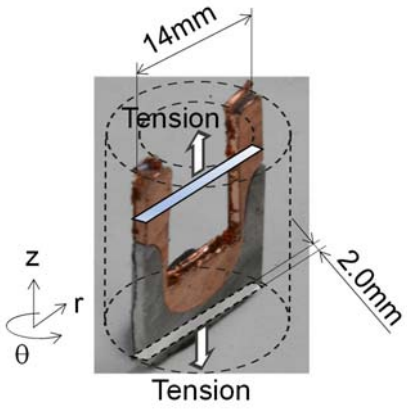

Fig. 2 Photograph of forge-bonded workpiece (upper part: copper, lower part: aluminum) sliced for uniaxial tensile test.

2.3. Measurement methods for sliding distance and bonded length

The relative circumferential sliding distance at the contact interface of the forge-bonded upper and lower workpieces was characterized from the circumferential sliding angle and the diameter of the workpiece. The circumferential sliding angle was measured by the angle between the two lines scribed on the outer surfaces of the upper and lower workpieces in experiment.

The bonded interface length of the forge-bonded workpieces in the extrusion direction was evaluated by the total machined depth in the z direction. The forge-bonded workpieces were sliced to a thickness of 2.0 mm in the center of the rθ cross section along the z-axis. Here, this slice was the same with that of the workpiece for tensile test as described in Section 2.2. Then the sliced workpiece was machined at a pitch of 0.5 mm in the z direction from the bottom of the forge-bonded lower workpiece. The machining of the lower workpiece was repeated until the separation from the upper workpiece. If the forge-bonded workpieces were separated at the *i*-th machining as shown in **Figure 3**, the total machined depth in the z direction was 0.5*i*. The bonded length of the sliced forge-bonded workpiece was calculated from the total machined depth and the geometrical profile of the bonded interface.

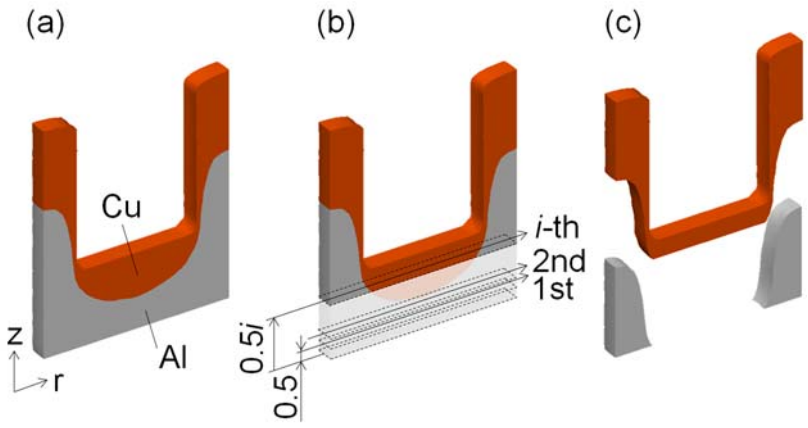

Fig. 3 Schematic illustrations of machining for measurement of bonded area of forge-bonded workpiece: (a) sliced workpiece, (b) *i*-th machining, (c) separation of upper and lower workpieces after *i*-th machining (total machined depth 0.5*i* mm).

2.4. Finite element analysis conditions

To investigate the torsion and circumferential sliding of the workpieces during forge-bonding with circumferential sliding, plastic deformation of the workpieces was calculated using a commercial three-dimensional finite element analysis code, DEFORM-3D ver. 11.3 (Scientific Forming Technologies Corporation). The isothermal deformation was assumed in the analysis, since the temperature increase of the workpiece by plastic deformation was preliminary calculated to be maximum of 5 K under forge-bonding conditions. On the other hand, the dies were treated as rigid bodies under isothermal state.

Each workpiece was meshed by approximately 32000 tetrahedral 4-node elements. When the interference between the elements was deformed to be longer than 0.7 in the relative length (interferential length/element size), the elements were automatically remeshed to tetrahedral 4-node elements.

The flow stress of the workpieces was assumed to be isotropic hardening. **Figure 4** indicates the flow stresses of C1100 copper and A1070 aluminum used in the analysis. The

flow stresses were measured by the upsettability test with an initial strain rate of 2.4×10^{-2} s^{-1} at room temperature. According to the Swift law, the flow stress–strain relationships of the copper and aluminum in **Figure 4** were numerically fit as shown in the following equations.

$$\text{(C1100)} \qquad \sigma = 431(\varepsilon + 0.01)^{0.39} \qquad \text{(MPa)} \qquad (1)$$

$$\text{(A1070)} \qquad \sigma = 140(\varepsilon + 0.01)^{0.19} \qquad \text{(MPa)} \qquad (2)$$

Note that the knurled grooves on the end face of the punches were not included in the analysis, since the punch–workpiece interface was assumed to be sticking (no sliding). For the side face of punch–workpiece and the container–workpiece interfaces with lubrication, the coefficients of friction were set to $\mu = 0.1$ on assumption of the Coulomb's friction law. As for the upper–lower workpiece interface, the friction state was expected to change during forge-bonding process. However, the coefficient and the change in the coefficient during forge-bonding were difficult to be explicitly identified. Hence, the coefficients of friction were set to $\mu_i = 0$, 0.05, 0.1 and assumed to be sticking.

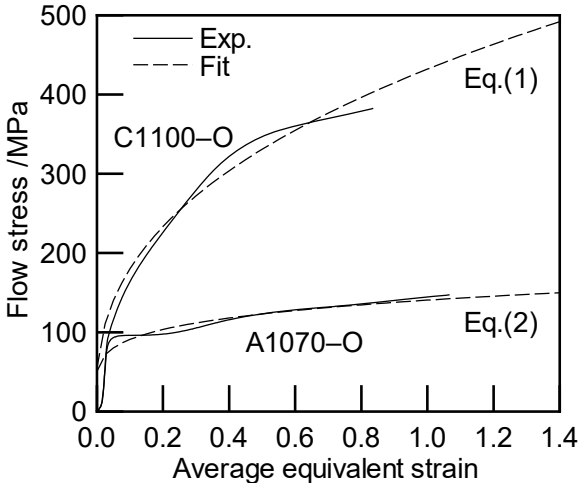

Fig. 4 Flow stress curves of C1100-O copper and A1070-O aluminum measured by the upsettability test at room temperature.

3. Finite element analysis results of torsion and circumferential sliding of workpieces

Figure 5 shows the calculated distribution of the circumferential speed of the upper and lower workpieces in forge-bonding with circumferential sliding. With regards to the lower workpiece, the circumferential speed increased in the radial direction and decreased in the height direction. As the result, the lower workpiece was twisted. The decrease in the circumferential speed became greater as the coefficient of friction on the upper–lower workpiece interface increased. As for the upper workpiece, the bottom was hardly twisted and rotated, while the sidewall was slightly rotated in the circumferential direction. Both torsion and rotation decreased as the coefficient of friction on the upper–lower workpiece interface increased. However, the decrease was much smaller than that of the lower workpiece. At the contact interface of the upper and lower workpieces, the circumferential speed was discontinuously changed. This change was a result of relative circumferential sliding. The sliding speed increased with the decrease of the coefficient of friction on the upper–lower workpiece interface. The change of the sliding speed was small in the radial direction.

Figure 6 shows the calculated and measured relative circumferential sliding distances between the upper and lower workpieces at the contact interface during forge-bonding. The experimentally measured sliding distance at the outer surface of the upper and lower workpieces agreed to the calculated sliding distance with μ_i = 0.05 at s = 4.0 mm and 6.0 mm. The sliding distance with ω = 0.5 rpm increased with the increase of the forging stroke.

From the above analysis results, circumferential sliding was confirmed to be given by the circumferential rotation of the lower punch during forge-bonding with circumferential sliding.

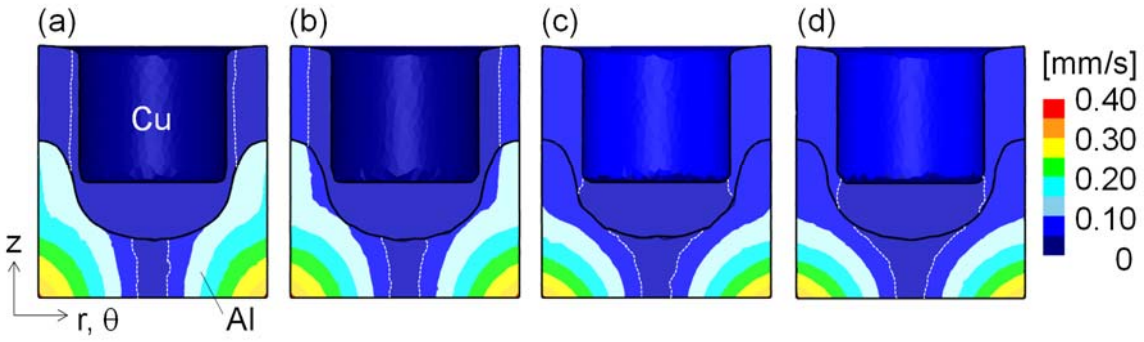

Fig. 5 Calculated distribution of circumferential speed of upper and lower workpieces in forge-bonding with circumferential sliding (ω = 0.5 rpm) under several coefficients of friction at upper–lower workpiece interface: (a) μ_i = 0, (b) μ_i = 0.05, (c) μ_i = 0.1, (d) sticking.

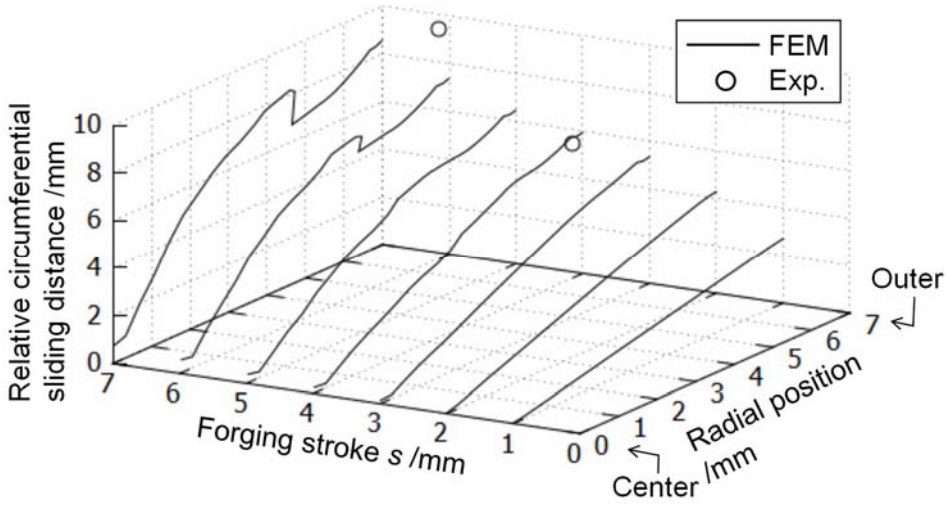

Fig. 6 Calculated and measured relative circumferential sliding distances between upper and lower workpieces at contact interface during forge-bonding with circumferential sliding (ω = 0.5 rpm, μ_i = 0.05).

4. Experimental results

4.1. Forging load and torque

The experimental results of the forging pressure and the torque during forge-bonding are shown in **Figure 7**. Here, the forging pressure was identified by dividing the forging load

with the rθ cross-sectional area of the land part of the upper punch (ϕ9.0 mm). From the consideration of the analysis results in Section 3, the lower workpiece was circumferentially rotated and twisted by the rotation of the lower punch, because the torque increased from the early stage of forge-bonding with ω = 0.5 rpm. Due to the superposition of axial compression and circumferential torsion, the forging pressure in forge-bonding with ω = 0.5 rpm was reduced by approximately 10%. This 10% reduction is equivalent to torsion with ω = 0.17 rpm, since the forging pressure was experimentally reduced by approximately 7% with ω = 0.1 rpm and 14% with 0.25 rpm, in upsetting with grooved dies (Matsumoto et al., 2017).

From the above experimental results, torsion of the lower workpiece and circumferential sliding at upper–lower workpiece interface are found to be caused during forge-bonding with circumferential sliding.

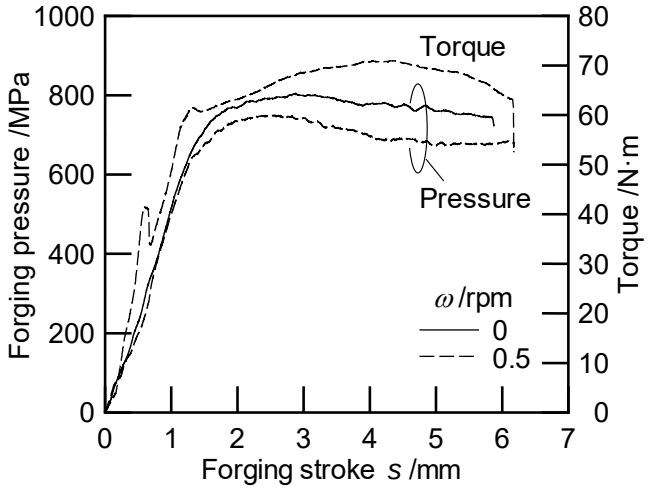

Fig. 7 Experimental results of forging pressure and torque in forge-bonding with circumferential sliding.

4.2. Relationship between forge-bonding conditions and bonding state

Figure 8 shows the appearances of the upper and lower workpieces after forge-bonding. Here, **Figures 8(b)-(d)** are the photographs of the sliced workpieces. The

bonding states of the upper and lower workpieces after forge-bonding were classified into four types; no bonding (**Figure 8(a)**), separation (no bonding) during slicing along the z-axis (bonding before slicing) (**Figure 8(b)**), successfully bonding (**Figure 8(c)**) and bonding with rupture of the upper workpiece sidewall during forge-bonding (**Figure 8(d)**). In **Figure 8(b)**, bonding of the upper and lower workpieces before slicing was due to either mechanical joining (anchor effect) of the interface shape or clamping force of the lower workpiece on the upper workpiece in the radial direction.

Figure 9 describes the bonding states of the upper and lower workpieces after forge-bonding in the map of cumulative rotation angle of the lower punch and forging stroke of the upper punch. The sliced workpieces after forge-bonding were used to assess the state of bonding. The workpieces were bonded at $s \geq 6.9$ mm in forge-bonding with $\omega = 0$ rpm, while they were bonded at $s \geq 5.3$ mm in forge-bonding with $\omega = 0.5$ rpm. The combination of circumferential sliding shortened the forging stroke for bonding. For example, the forging stroke for bonding was shortened by approximately 25% with $\omega = 0.5$ rpm of circumferential sliding.

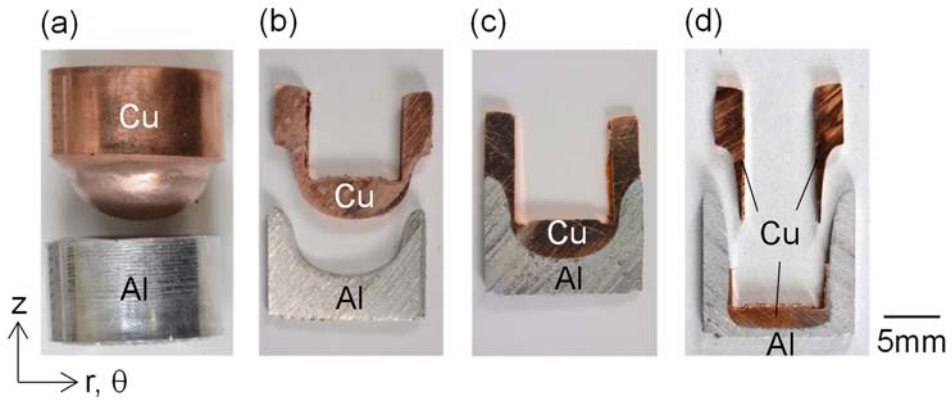

Fig. 8 Bonding states of upper and lower workpieces after forge-bonding with circumferential sliding: (a) no bonding (s = 4.4 mm with ω = 0 rpm), (b) separation during slicing (bonding before slicing) (s = 6.7 mm with ω = 0 rpm), (c) bonding (s = 6.7 mm with ω = 0.5 rpm), (d) bonding with rupture of upper workpiece during forge-bonding (bonding) (s = 9.1 mm with ω = 0.5 rpm).

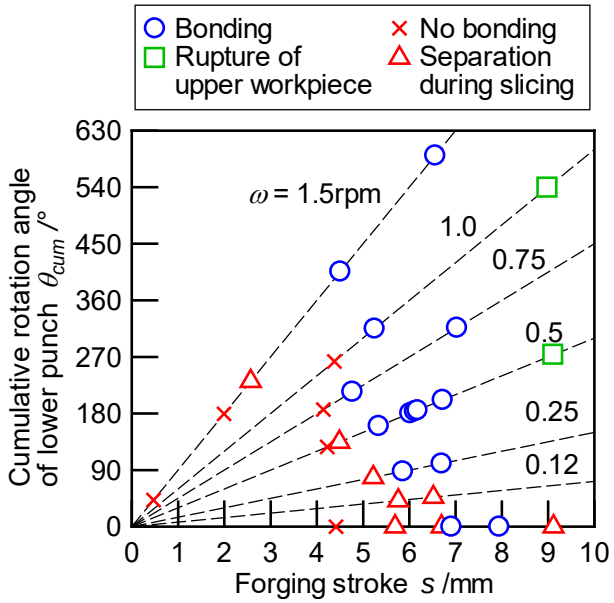

Fig. 9 Relationship between bonding states of forge-bonded workpiece and forge-bonding conditions.

4.3. Bonding strength

The nominal tensile stress–stroke curves of the forge-bonded workpiece in uniaxial tensile test are shown in **Figure 10**. The upper workpiece was pulled to either separation from the lower workpiece or rupture at the sidewall. **Figure 11** shows the measured bonding strength (maximum nominal tensile stress in tensile test) of the forge-bonded workpiece under typical forge-boning conditions. The bonding strength of the workpieces which were forge-bonded at minimum forging stroke with each rotation speed (s = 6.9 mm with ω = 0 rpm, s = 5.3 mm with ω = 0.5 rpm) was approximately 3 MPa. In these cases, the forge-bonded workpiece was separated at the upper–lower workpiece interface during the tensile test. The maximum bonding strength was approximately 4 MPa at s = 7.9 mm with ω = 0 rpm, and 16 MPa at s = 6.9 mm with ω = 0.5 rpm. The upper–lower workpiece interface forge-bonded at s = 6.9 mm with ω = 0.5 rpm is predicted to have higher bonding strength. This is because the sidewall of the upper workpiece was ruptured during the tensile test, while the interface still remained bonded together.

The bonded interface length in the extrusion direction was estimated from the machined depth of the forge-bonded lower workpiece (see Section 2.3). The total machined depths at s = 6.9 mm were 4.0 mm with ω = 0 rpm, and 4.5 mm with ω = 0.5 rpm. The bonded length of the sliced forge-bonded workpiece was estimated to be approximately 10 mm in the radial direction. Since the bonded length in the radial direction was close to the upper punch diameter (ϕ9.0 mm), the bonded area was limited to the contact interface located below the upper punch. From the comparison of the bonded length and the workpiece diameter, the true bonding strength has a potential of being approximately 1.4 times higher than the nominal bonding strength.

Figure 12 shows the measured nominal bonding strength of the upper and lower workpieces plotted in the map of cumulative rotation angle and forging stroke. Here, the

bonding strength of the upper workpiece which ruptured before the tensile test was not measured, because it could not be gripped on the material testing machine. In addition, where no bonding was obvious, the nominal bonding strength was set to 0 MPa in the forge-bonding conditions; for example, s = 0 mm with ω = 0 rpm. The nominal bonding strength increased with the increases of forging stroke and rotation angle. The maximum nominal bonding strength was approximately 30 MPa at s = 6.6 mm with ω = 1.5 rpm (θ_{cum} = 590°), as shown in **Figure 12**.

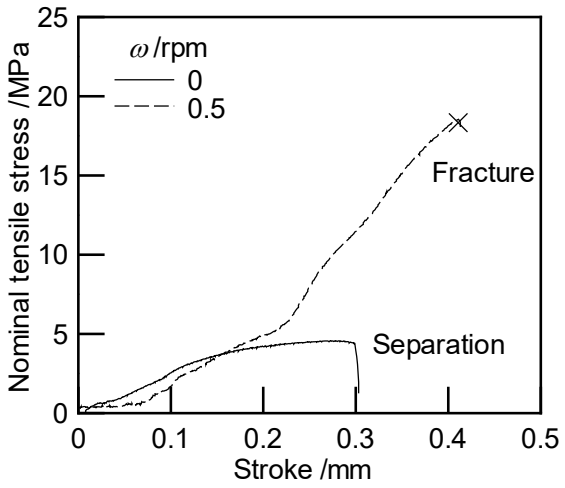

Fig. 10 Nominal tensile stress–stroke curves of forge-bonded workpiece in uniaxial tensile test (s = 6.9 mm).

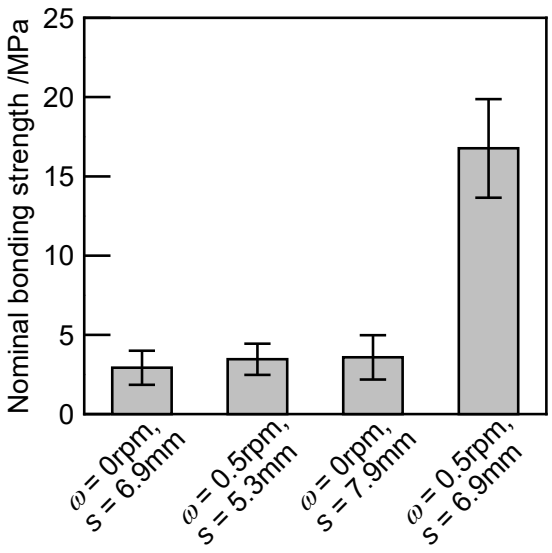

Fig. 11 Nominal bonding strength of forge-bonded workpiece in uniaxial tensile test.

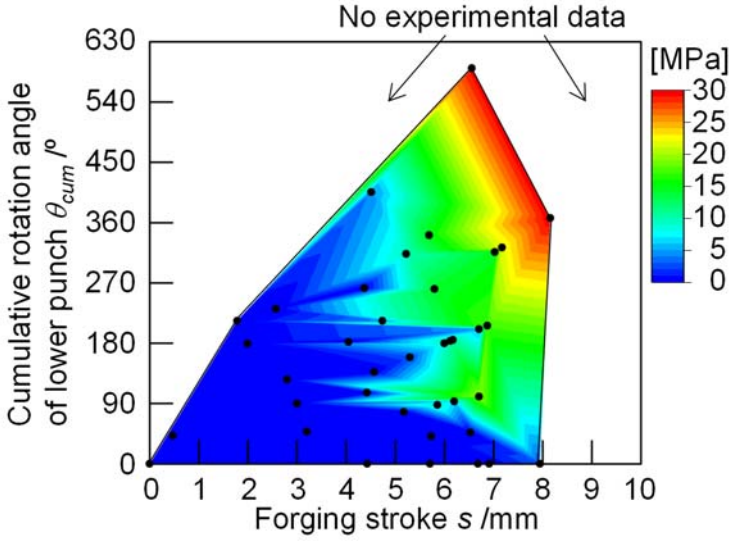

Fig. 12 Relationship between nominal bonding strength of forge-bonded workpiece and forge-bonding conditions.

5. Discussions of bonding mechanism

5.1. Bonding factors in cold forge-bonding

Bonding factors of the workpieces in cold forge-bonding without circumferential sliding (with $\omega = 0$ rpm) are listed as follows:

(a) Pressure welding due to forging pressure.

(b) Mechanical joining (anchor effect) due to macroscopic and microscopic geometrical profiles of contact interface.

(c) Clamping force between upper and lower workpieces due to residual stress of workpieces in radial direction.

(d) Diffusion of copper and aluminium due to heat generation by plastic deformation.

(e) Formation of virgin surface without oxide by plastic deformation at contact interface.

The forging pressure which depends on the forging stroke was kept to approximately 750–800 MPa at $s \geq 2.0$ mm. However, the workpieces were not bonded at $s < 6.9$ mm in forge-bonding with $\omega = 0$ rpm (see **Figures 7 and 9**). The normal pressure at the contact interface between upper and lower workpieces is difficult to be predicted from the forging pressure. However, it generally tends to be lower than the forging pressure. Hence, forging pressure is one of the necessary bonding factors, but not the only factor in forge-bonding ((a)). The upper workpiece was partly covered with the lower workpiece in the sidewall of the forge-bonded workpiece (see **Figure 8**). Macroscopic geometry of the contact interface of the forge-bonded workpieces was convex to the forge-bonded lower workpiece (see **Figure 13**). The surface roughness of the contact interface of the forge-bonded workpieces was $Ra < 4$ μm with/without circumferential sliding. From the considerations of the macroscopic and microscopic geometrical profiles, the forge-bonded workpieces are not mechanically joined ((b)).

In addition, the contact interface was bonded after slicing of the forge-bonded workpieces in rz cross-section, except for the early stage of bonding at each rotation speed of the lower punch (see **Figures 8(b) and 9**). Thus, the clamping force between the forge-bonded upper and lower workpieces is predicted to be small ((c)). Since the temperature increase of the workpieces at the contact interface during cold forge-bonding was predicted to

be maximum of 5 K by the finite element analysis, diffusion of the workpieces does not occur at the contact interface ((d)).

From considerations of the shapes of the initial and forge-bonded workpieces, the nominal surface expansion ratio of the bottom surface area of the forge-bonded upper workpiece was estimated to roughly 1.1–1.3 at s = 4.6 mm (see **Figure 13**). Here, the nominal surface expansion ratio was calculated by dividing the difference of the bottom surface areas of the forge-bonded and initial upper workpieces with the initial bottom surface area of the upper workpiece. On the other hand, bonding of aluminium on copper was slightly detected in the forge-bonded workpieces by energy dispersive x-ray spectroscopy (EDS) analysis (see **Figure 14**). Bonding due to surface expansion is one of the bonding factors, however, considering the amount of bonding, the bonding strength is expected to be low ((e)).

From the above discussions, forging pressure (forging stroke) and surface expansion (bonding of aluminium) are concluded to be the main bonding factors of the workpieces in cold forge-bonding with ω = 0 rpm. The bonding area of the workpieces is limited below the upper punch. Thus, the bonding state of this forge-bonding process is similar with that of the cold spot pressure welding. The bonding strength of the copper and aluminum in other cold forge-bonding processes was reported as 5–50 MPa in cold pressure welding (Ohashi and Hashimoto, 1978), 20–180 MPa in cold forward-backward extrusion (Yoshida et al., 2012a) and 10–140 MPa in cold upsetting (Azad et al., 2015). The bonding strength in this study (approximately 4 MPa) was overall lower than that of the above processes. The forge bonding conditions such as extrusion ratio, extrusion shape and initial workpiece heights, may not be appropriated for strong bonding of the workpieces.

5.2. Improvement mechanism of bondability by applying circumferential sliding

As described in Section 4.1, circumferential sliding reduced the forging pressure by

approximately 10% in forge-bonding with ω = 0.5 rpm. Nakamura et al. (1990) reported that the real contact area of JIS: A1050-O aluminium was nearly 100% under contact pressure higher than 200 MPa with surface sliding longer than 0.25 mm. In this study, it is concluded that the reduction in the forging pressure did not reduce the real contact area of the upper and lower workpieces. This is because (1) the forging pressure (approximately 750–800 MPa) was much higher than 200 MPa and (2) the relative sliding along the forging direction was caused at the contact surface of the upper and lower workpieces in this forge-bonding with/without circumferential sliding.

Figure 13 shows the shape measurement results of the contact interface of the forge-bonded upper workpiece (copper). The shapes of the contact interface were almost the same with ω = 0 rpm and 0.5 rpm. The profile and surface expansion ratio were not changed by applying circumferential sliding. The bonded interface area with ω = 0.5 rpm is predicted to be slightly larger than that with ω = 0 rpm as mentioned in Section 4.3.

Figure 14 shows the line element analysis results on the rz cross-section of the bonded interface of the forge-bonded workpieces. The element intensity was obtained by energy dispersive x-ray spectrometry (EDX) analysis. The width detected with both copper and aluminum was approximately 2 μm around the contact interface with ω = 0 rpm and 0.5 rpm. **Figure 15** shows the element map of the contact interface for the forge-bonded upper workpiece (copper). At the radial position of 4.5 mm, aluminum was slightly detected with area fraction of aluminum α = 0.11–0.12 in the workpiece with ω = 0 rpm, while aluminum was detected with α = 0.24–0.29 in the workpiece with ω = 0.5 rpm. The detected area of aluminum increased by 2.1–2.5 times. On the other hand, the detected area of aluminum was small with $\alpha \leq 0.14$ in the workpieces with ω = 0 rpm and 0.5 rpm at the radial position of 0 mm (radial center). However, the detected area slightly increased in the workpiece with ω = 0.5 rpm. This is because the relative sliding at the contact interface between the upper and

lower workpieces was small around the radial center.

Using the experimental results of **Figure 12**, relationship between the nominal bonding strength and the relative circumferential sliding distance is plotted in **Figure 16**. Here, the relative circumferential sliding distance of the workpiece was estimated from both the forging stroke and the rotation angle of the lower punch on the following assumptions. It is assumed that torsion occurs mostly in the lower workpiece as described in Section 3. The torsion speed of the lower workpiece was estimated from the reduction for forging load without torsion as described in Section 4.1. The relative circumferential sliding distance was calculated at the radial position of 3.5 mm. This is because the relationship between the circumferential sliding distance and the radial position of the workpiece was almost linear as shown in **Figure 6**. The bonding strength sharply increased at sliding distance of 5–15 mm. Ohashi and Hashimoto (1978) reported that the increase of the relative circumferential sliding distance of 2–10 mm improved the bonding strength by 20–40 MPa in cold pressure welding with copper and aluminum under normal interface pressure of 100–200 MPa. This was mainly due to increases in surface expansion and seizure. The circumferential sliding distance in the above report almost agrees to the circumferential sliding distance in **Figure 16**.

Based on the above, it is concluded that the main bonding factors (forging pressure and surface expansion) are the same with/without circumferential sliding. Both the geometrical profile and surface expansion ratio of the contact interface between the upper and lower workpieces were not changed by applying circumferential sliding. On the other hand, bonding of the lower workpiece (aluminum) on the upper workpiece (copper) was promoted by applying circumferential sliding.

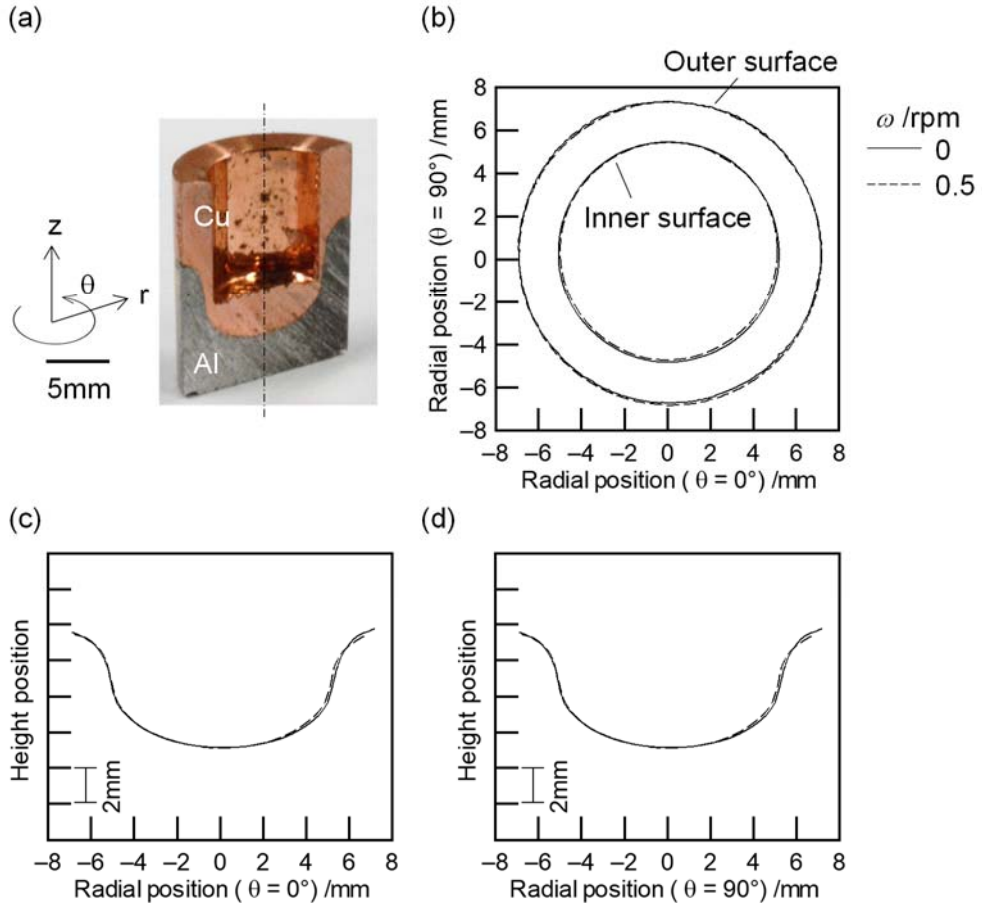

Fig. 13 Shape of contact interface of forge-bonded upper workpiece (copper) (s = 4.6 mm): (a) appearance of rz cross-section of forge-bonded workpiece, (b) rθ cross-section (z = 6.0 mm), (c) rz cross-section (θ = 0°), (d) rz cross-section (θ = 90°).

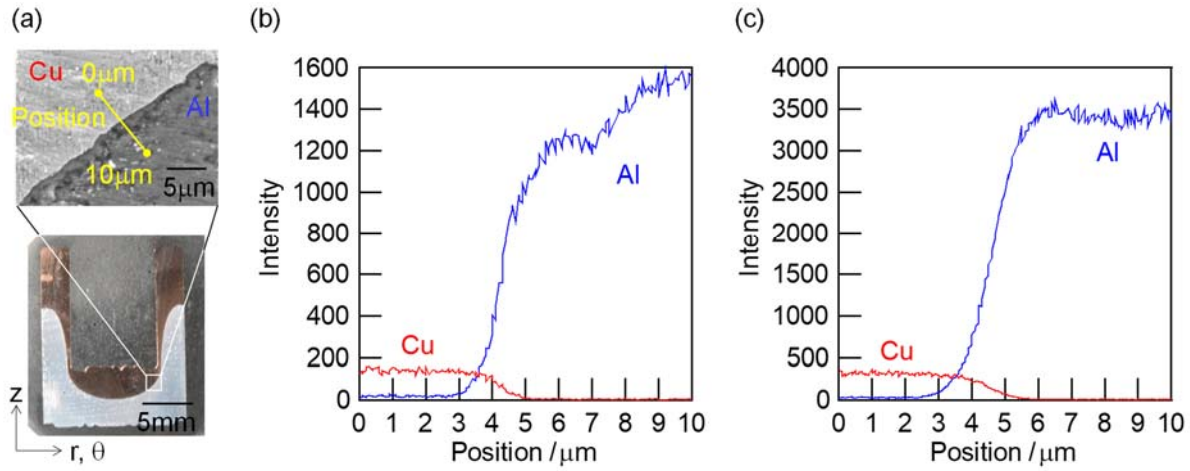

Fig. 14 Element intensity on bonded interface of forge-bonded workpieces (s = 6.4 mm): (a) analyzed area, (b) ω = 0 rpm, (c) ω = 0.5 rpm.

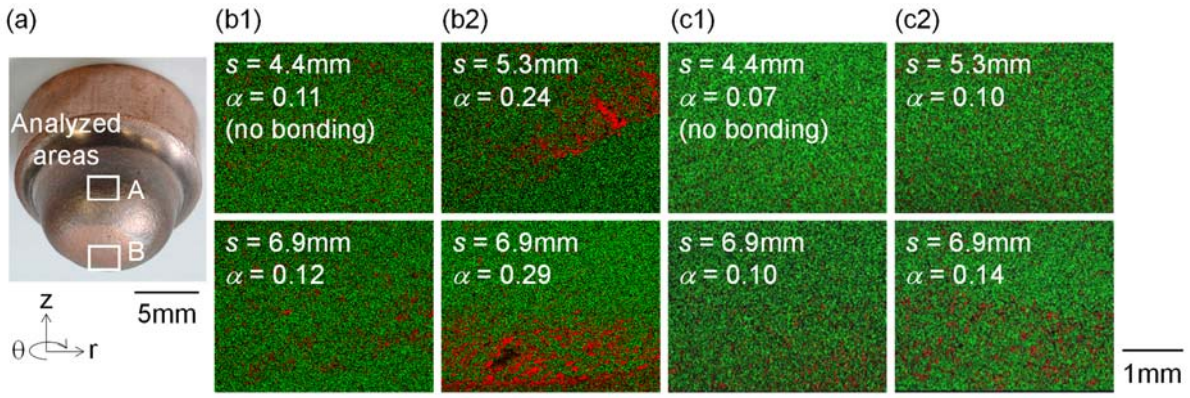

Fig. 15 Element maps on contact interface of forge-bonded upper workpiece (copper) by EDX (red: aluminum, green: copper, α: detected area fraction of aluminum): (a) analyzed areas (radial position: 4.5 mm (area A), 0 mm (area B)), (b) area A (b1: ω = 0 rpm, b2: ω = 0.5 rpm), (c) area B (c1: ω = 0 rpm, c2: ω = 0.5 rpm).

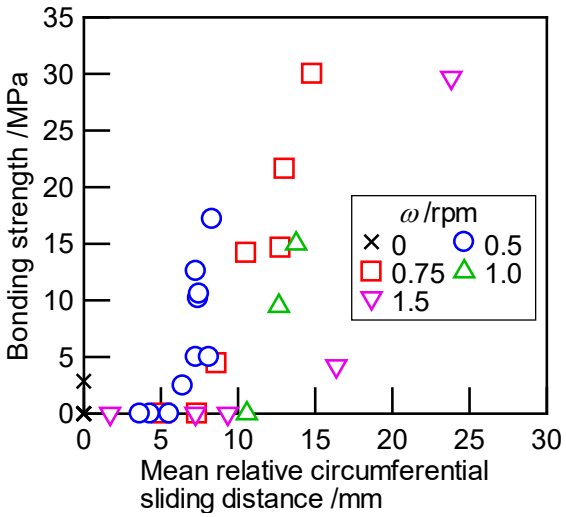

Fig. 16 Relationship between nominal bonding strength of forge-bonded workpiece and relative circumferential sliding distance in forge-bonding with circumferential sliding.

6. Conclusions

In this study, the effects of circumferential sliding on bonding characteristics of

copper and aluminum workpieces at the contact interface were investigated by the experiment of cold forge-bonding process. Two stacked cylindrical workpieces were backward-extruded into a cup shape by an upper punch in the forging direction. Simultaneously the workpieces were rotated by a lower punch with respect to the forging axis in forge-bonding process (maximum forging stroke of the upper punch: 9.1 mm, maximum rotation angle of the lower punch: 590°). The following conclusions were obtained.

(1) Main bonding factors are forging pressure and surface expansion of the contact interface in this forge-bonding process with/without circumferential sliding.

(2) Circumferential sliding on the contact interface of the upper and lower workpieces was given by the circumferential rotation of the lower punch.

(3) The combination of circumferential sliding with forging deformation shortened the forging stroke for bonding. For example, the forging stroke for bonding was shortened by approximately 25% in circumferential sliding with rotation speed of the lower punch of 0.5 rpm.

(4) The bonding strength increased with the increases of the forging stroke and rotation angle. The maximum nominal bonding strength was approximately 30 MPa at a forging stroke of 6.6 mm with rotation speed of 1.5 rpm (rotation angle of 590°).

(5) The improvement in bonding characteristics by applying circumferential sliding was mainly due to the increase of bonding of the aluminum workpiece on the copper workpiece. The bonding area of aluminium increased by 2.1–2.5 times at the contact interface of the workpieces forge-bonded with rotation speed of 0.5 rpm.

Acknowledgements

This study was financially supported in part by the Amada Foundation (AF-2019007-B2) and the Light Metal Educational Foundation, Inc.

References

- Azad, M.R., Ghasemi, A., Pouraliakbar, H., Jandagh, M.R., 2015, On the Al/Cu dissimilar joints produced through simple cold compression. Transactions of the Indian Institute of Metals. 68(5), 991-998. [doi: 10.1007/s12666-014-0496-2]
- Bay, N., 1979, Cold pressure welding – The mechanisms governing bonding. Transactions of the ASME: Journal of Engineering for Industry. 101(2), 121-127. [doi: 10.1115/1.3439484]
- Bay, N., Bjerregaard, H., Petersen, S.B., Santos, C.H.G., 1994, Cross shear roll bonding. Journal of Materials Processing Technology. 45(1-4), 1-6. [doi: 10.1016/0924-0136(94)90309-3]
- Cai, W., Daehn, G., Vivek, A., Li, J., Khan, H., Mishra, R.S., Komarasamy, M., 2019, A state-of-the-art review on solid-state metal joining. Transactions of the ASME: Journal of Manufacturing Science and Engineering. 141(3), 031012. [doi: 10.1115/1.4041182]
- Groche, P., Wohletz, S., Brenneis, M., Pabst, C., Resch, F., 2014, Joining by forming – A review on joint mechanisms, applications and future trends. Journal of Materials Processing Technology. 214(10), 1972-1994. [doi: 10.1016/j.jmatprotec.2013.12.022]
- Groche, P., Wohletz, S., Erbe, A., Altin, A., 2014, Effect of the primary heat treatment on the bond formation in cold welding of aluminum and steel by cold forging. Journal of Materials Processing Technology. 214(10), 2040-2048. [doi: 10.1016/j.jmatprotec.2013.12.021]
- Klaus, M., Merklein, M., 2020, Potential of joining dissimilar materials by cold formed pin-structures. Journal of Materials Processing Technology. 283, 116697. [doi: 10.1016/j.jmatprotec.2020.116697]
- Martinsen, K., Hu, S.J., Carlson, B.E., 2015, Joining of dissimilar materials. CIRP Annals

– Manufacturing Technology. 64(2), 679-699. [doi: 10.1016/j.cirp.2015.05.006]

- Matsumoto, R., Kou, J., Utsunomiya, H., 2017, Reduction in axial forging load by low-frequency torsional oscillation in cold upsetting. International Journal of Advanced Manufacturing Technology. 93(1-4), 933-943. [doi: 10.1007/s00170-017-0553-1]
- Miwada, Y., Ishiguro, T., Abe, E., Yukawa, N., Ishikawa, T., Suganuma, T., 2014, Cold forge spot-bonding of high tensile strength steel and aluminum alloy sheets. Procedia Engineering. 81, 2006-2011. [doi: 10.1016/j.proeng.2014.10.272]
- Mori, K., Bay, N., Fratini, L., Micari, F., Tekkaya, A.E., 2013, Joining by plastic forming. CIRP Annals – Manufacturing Technology. 62(2), 673-694. [doi: 10.1016/j.cirp.2013.05.004]
- Nakamura, T., Kondo, K., Nishigaya, T., 1990, Smoothing conditions of workmetal surface in metalworking processes: effects of contact pressure and relative slip displacement. Transactions of the Japan Society of Mechanical Engineers Series C. 56(530), 2794-2801. (in Japanese) [doi: 10.1299/kikaic.56.2794]
- Napierala, O., Dahnke, C., Tekkaya, A.E., 2019, Simultaneous deep drawing and cold forging of multi-material components: Draw-forging. CIRP Annals – Manufacturing Technology. 68(1), 269-272. [doi: 10.1016/j.cirp.2019.03.001]
- Ohashi, O., Hashimoto, T., 1978, The effects of sliding along interface and anodic oxidation on cold welding of aluminum-aluminum and aluminum copper. Journal of the Japan Welding Society. 47(5), 294-299. (in Japanese) [doi: 10.2207/qjjws1943.47.294]
- Plancak, M., Vilotic, D., Car, Z., Movrin, D., Kacmarcik, I., Krsulja, M., 2012, Forward extrusion of bi-metallic components. Proceedings of 4th International Scientific and Expert Conference of the International TEAM Society. 125-128.
- Yoshida, Y., Ishikawa, T., Suganuma, T., 2012a, Processing property of backward extrusion forged bonding in non-ferrous metals. Proceedings of the 63rd Japanese Joint

Conference for the Technology of Plasticity. 265-266. (in Japanese)

- Yoshida, Y., Matsubara, T., Yasui, K., Ishikawa, T., Suganuma, T., 2012b, Influence of processing parameters on bonding conditions in backward extrusion forged bonding. Key Engineering Materials. 504-506, 387-392. [doi: 10.4028/www.scientific.net/KEM.504-506.387]
- Zebardast, M., Taheri, A., 2011, The cold welding of copper to aluminium using equal channel angular extrusion (ECAE) process. Journal of Materials Processing Technology. 211(6), 1034-1043. [doi: 10.1016/j.jmatprotec.2011.01.004]